

Integrative Proteomic and Metabolomic Analysis Reveals Metabolic Phenotype in Mice With Cardiac-Specific Deletion of Natriuretic Peptide Receptor A

Authors

Pan Chang, Yan Niu, Xiaomeng Zhang, Jing Zhang, Xihui Wang, Xi Shen, Baoying Chen, and Jun Yu

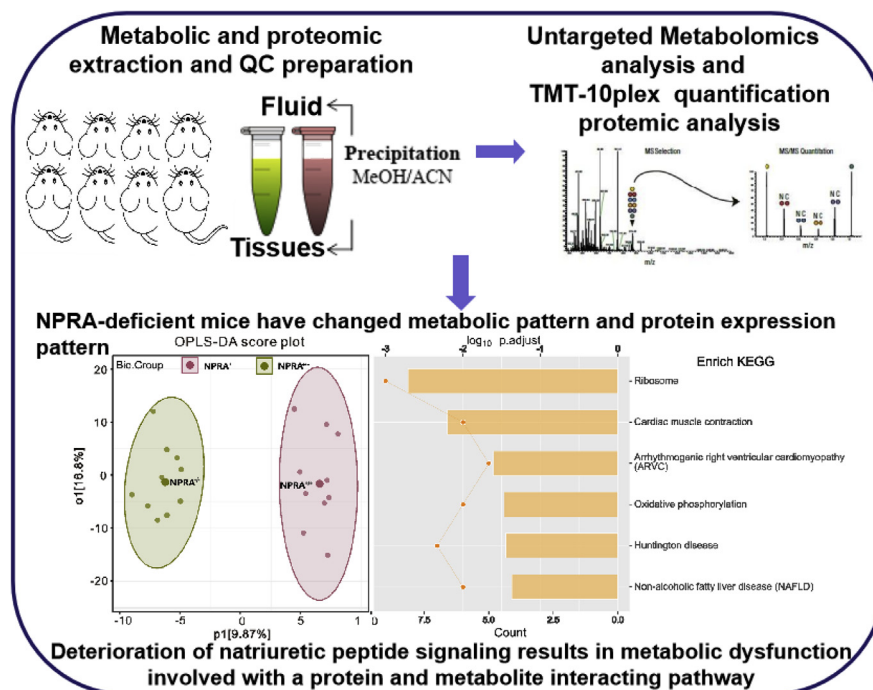
Correspondence

chenby128@163.com;
pclamper@163.com

In Brief

Metabolomic analysis in mice revealed that natriuretic peptide receptor A (NPRA) is mainly involved in nucleotide biosynthesis and histidine metabolism in cardiac tissues, and in creatine metabolism, TCA cycle and pentose phosphate pathway in the plasma. Furthermore, proteomics revealed that Cox7c, Cox7b, ATP5J2, Uqcrl0, and Myh7 play a vital role in the regulation of metabolic pathway. Together, deterioration of NPRA results in metabolic dysfunction involved with a protein and metabolite-interacting pathway.

Graphical Abstract



Highlights

- Metabolomic analysis of cardiac tissues from NPRA-deficient mice.
- Metabolomic analysis of plasma from NPRA-deficient mice.
- TMT-based proteomic analysis of cardiac tissues in NPRA-deficient mice.
- Mechanistic insights into NPRA in mice from metabolomes and proteomes.

Integrative Proteomic and Metabolomic Analysis Reveals Metabolic Phenotype in Mice With Cardiac-Specific Deletion of Natriuretic Peptide Receptor A

Pan Chang^{1,‡}, Yan Niu^{2,‡} , Xiaomeng Zhang^{2,‡}, Jing Zhang¹, Xihui Wang¹, Xi Shen², Baoying Chen^{3,*}, and Jun Yu^{2,*}

Atrial natriuretic peptide (ANP) and brain natriuretic peptide (BNP) are important biological markers and cardiac function regulators. Natriuretic peptide receptor A (NPRA) binds to an ANP or BNP ligand and induces transmembrane signal transduction by elevating the intracellular cyclic guanosine monophosphate (cGMP) levels. However, the metabolic phenotype and related mechanisms induced by NPRA deletion remain ambiguous. Here, we constructed myocardial-specific NPRA deletion mice and detected the heart functional and morphological characteristics by histological analysis and explored the altered metabolic pattern and the expression patterns of proteins by liquid chromatography–mass spectrometry (LC-MS)-based omics technology. NPRA deficiency unexpectedly did not result in significant cardiac remodeling or dysfunction. However, compared with the matched littermates, NPRA-deficient mice had significant metabolic differences. Metabolomic analysis showed that the metabolite levels varied in cardiac tissues and plasma. In total, 33 metabolites were identified in cardiac tissues and 54 were identified in plasma. Compared with control mice, NPRA-deficient mice had 20 upregulated and six downregulated metabolites in cardiac tissues and 25 upregulated and 23 downregulated metabolites in plasma. Together, NPRA deficiency resulted in increased nucleotide biosynthesis and histidine metabolism only in heart tissues and decreased creatine metabolism only in plasma. Further proteomic analysis identified 136 differentially abundant proteins in cardiac tissues, including 54 proteins with higher abundance and 82 proteins with lower abundance. Among them, cytochrome c oxidase subunit 7c and 7b (Cox7c, Cox7b), ATP synthase, H⁺ transporting, mitochondrial Fo complex subunit F2 (ATP5J2), ubiquinol-cytochrome c reductase, complex III subunit X (Uqcrl10), and myosin heavy chain 7 (Myh7) were mainly involved in related metabolic pathways. These results revealed the

essential role of NPRA in metabolic profiles and may elucidate new underlying pathophysiological mechanisms of NPRA in cardiovascular diseases.

Atrial natriuretic peptide (ANP) and brain natriuretic peptide (BNP) are well-known cardiovascular hormones of the mammalian natriuretic peptide (NP) system produced by atrial granules of the heart in response to myocardial stretch (1). All NPs have pleiotropic cardiometabolic protective effects, including natriuresis, diuresis, vasodilation, lusitropy, lipolysis, weight loss, improved insulin sensitivity, and antagonism of the renin–angiotensin system (2).

Cardiovascular diseases continue to be the leading cause of morbidity and mortality worldwide. NPs play a key role in cardiovascular protection. NPs exert their functions by interacting with their cell surface receptors (3). Natriuretic peptide receptor A (NPRA), also called NPR1, or guanylyl cyclase-A (GC-A), is a particulate guanylyl cyclase that catalyzes the synthesis of cyclic guanosine monophosphate (cGMP) when bound to ANP or BNP. Activation of NPRA by ligand binding results in elevated levels of the second messenger cGMP, which in turn mediates the physiological and pathophysiological processes via cGMP-dependent protein kinases (PKGs). Thus, ANP/BNP-NPRA-cGMP-PKG is a classical signaling pathway mediating the functions of various kinds of organs and tissues, including the hearts and blood vessels. Importantly, blunted NP signals participate in and act as molecular targets of novel therapeutic approaches to cardiometabolic disease. However, the underlying mechanisms are not well understood (4).

Metabolomics and proteomics reflect dynamic changes downstream of genomics and transcriptomics. The proteome reveals all protein and peptide expression information in the

From the ¹Department of Cardiology, the Second Affiliated Hospital, Xi'an Medical University, Xi'an, P.R. China; ²Clinical Experimental Center, and ³Imaging Diagnosis and Treatment Center, Xi'an International Medical Center Hospital, Xi'an, P.R. China

[‡]These authors contributed equally to this work.

*For correspondence: Jun Yu, pclamper@163.com; Baoying Chen, chenby128@163.com.

body (5). Moreover, metabolomic analysis provides a detailed analysis of the metabolic profile in the tissues or body fluids of living organisms to reveal changes in the metabolites and metabolic pathways that occur in the body under conditions such as disease or drug intervention (6, 7). Metabolomics and proteomics complement each other, and they can be used to conduct a more comprehensive systematic evaluation of physiological status, especially for clarifying pathogenesis and identifying biomarkers by using modern data analysis methods to understand the complex system as a whole. Multiomics techniques have importantly contributed to the study of altered networks or pathways of pathological or medical relevance. As a platform for omics research, LC-MS has been widely used in a variety of studies owing to its higher sensitivity in contrast to nuclear magnetic resonance (NMR) and superior detection, allowing the detection of thermally unstable compounds with high polarity without the need for derivatization, unlike gas chromatography–mass spectrometry (GC-MS) (8).

In this study, to determine the function of NPRA in metabolism, we analyzed the underlying changes in the proteome and metabolome in cardiac tissues and plasma of NPRA-deficient mice as well as the matched littermates. A systematic study was applied in terms of the relative metabolite abundances and relative expression pattern of proteins based on LC-MS to screen out the representative changes involved in the development of cardiovascular disease related to the deficiency of NP signals.

EXPERIMENTAL PROCEDURES

Experimental Design and Statistical Rationale

Our study is based on NPRA-deficient mice and the matched littermates. For metabolomics, we analyzed respectively 20 samples of cardiac tissues and plasma from the two groups. Then, we analyzed 10 samples of heart tissues from NPRA-deficient mice and the matched littermate for proteomic research. Full description of materials and methods is depicted as follows.

Animals

All experimental protocols included in this manuscript were approved by the local animal care committee. In the previous research of the group, we have obtained myocardial-specific NPRA knockout mice (9). So we used the mice with cardiomyocyte-specific deletion of NPRA (NPRA^{fllox/fllox}; Myh6-Cre mice) as in the previous study. And NPRA^{fllox/fllox} littermates without the Myh6-Cre transgene were used as control. Eight-week-old mice were used in the studies. The animals were housed in stainless steel metabolic cages with controlled humidity (40–60%) and temperature (23–27 °C) on a 12 h light/dark cycle. They were given free access to food and tap water.

Histopathological Examination

Cardiac tissue was fixed in 4% formalin before being embedded in paraffin. Serial sections of the embedded specimens were stained with hematoxylin and eosin with the standard protocol. Histopathological changes in cardiac tissues were randomly assessed.

Echocardiography

Echocardiography was performed using a Vevo 770 UBM system (VisualSonics) that possesses a single-element mechanical transducer with a centre frequency of 30 MHz and a frame rate of 30 Hz. The body temperature of the mice was maintained between 36 °C and 38 °C. The heart rate was maintained between 350 and 450 beats/min. After measurement, the cardiac output values, such as the left ventricular ejection fraction (LVEF) and left ventricular fractional shortening (LVFS), were calculated according to the guidelines accompanying the Vevo 770 UBM system.

RNA Isolation and Quantitative Real-Time PCR

To determine the cardiac mRNA expression of NPRA in mice, total RNA was extracted from the cardiac tissues by using TRIzol (Invitrogen). The cDNA was reverse-transcribed using Superscript II Reverse Transcriptase (TaKaRa). Real-time quantitative PCR was performed using TransStart™ SYBR-Green qPCR Supermix (TaKaRa) and the CFX96 Touch™ system (Bio-Rad). The real-time quantitative PCR conditions were predenaturation at 95 °C (30 s), denaturation at 95 °C (5 s), and annealing at 56 °C (30 s). The denaturation and annealing steps were repeated 40 times and then dissociated at 95 °C (15 s). The data were analyzed using the $\Delta\Delta\text{CT}$ method. Independent experiments were repeated at least three times. The mRNA expression levels of NPRA were normalized to those of β -actin. The primer sequences were as follows: NPRA, 5'-GGCTGTGAAACGTGTGAACC-3' (F); 5'-GTCGGTACAAGTCCCACAA-3' (R). β -actin, 5'-GCAGGATACGATGAGTCCG-3' (F); 5'-ACGCAGCTCAGTAACAGTCC-3' (R).

Western Blotting

For preparation of tissue lysates, cardiac tissues from mice were dissected and washed with ice-cold PBS and homogenized with RIPA buffer with 150 mmol/L NaCl as described in our previous study (10). Then, the tissue suspension was centrifuged at 4 °C and 20,000 g for 10 min. After adjusting the protein concentration, the lysates were boiled in SDS sample loading buffer for 5 min and separated by SDS–polyacrylamide gel electrophoresis. Gels were blotted on a polyvinylidene difluoride (PVDF) membrane (Immobilon P; Millipore, Bedford, MA, USA) and stained with the indicated primary antibodies anti-NPRA (1:500 dilution, LifeSpan BioSciences, Inc, Seattle, USA) and anti-GAPDH (40 ng/ml, Santa Cruz, Inc, Santa Cruz, CA, USA). Antibody binding was detected with horseradish peroxidase (HRP)-conjugated secondary antibodies followed by chemiluminescence detection (ECL Plus; Amersham Pharmacia, Uppsala, Sweden).

LC/MS-Based Metabolomic Analysis

Sample Preparation and Metabolite Extraction—Mice were humanely sacrificed under general anesthesia, and specimens of the heart were dissected immediately, frozen in liquid nitrogen, and stored at –80 °C until use. Blood samples were collected and centrifuged at 2000 rpm at 4 °C for 10 min to separate the plasma and then kept at –80 °C until analysis. Then, for the metabolites, the plasma samples were thawed and vortexed for 30 s, and sample volumes of 200 μ l were extracted with MeOH:ACN (1:1, v/v) and homogenized. Cardiac tissue was thawed and weighed, and then MeOH:ACN (1:1, v/v) was added to the samples, which were then vortexed for 30 s and sonicated for 10 min. For protein precipitation, the samples were incubated for 1 h at –20 °C, followed by 15 min centrifugation at 20,000 g and 4 °C. The resulting supernatant was removed and evaporated to dryness in a vacuum concentrator. The dry extracts were then reconstituted with ACN:H₂O (1:1, v/v) at 40 μ l/mg, vortexed for 30 s, homogenized, and sonicated for 10 min. The extracts were centrifuged for 15 min at 20,000 rpm and 4 °C to remove insoluble debris.

The supernatants were transferred to HPLC vials and stored at -80°C prior to LC/MS analysis.

QC samples were prepared by pooling 10 μl from each sample and used to assess the reproducibility and reliability of the UPLC-MS system. The QC sample extraction was conducted with the same method used for the sample preparation.

LC-MS/MS—Samples were separated on an amide column using mobile phase A consisting of water mixed with 25 mM ammonium acetate and 25 mM ammonium hydroxide and mobile phase B ACN. The injection volume was 4 μl , and the flow rate was 0.4 ml/min. MS analysis was carried out on the Q-Exactive MS/MS in both positive and negative ion modes. (1) The relevant tuning parameters for the probe were set as follows: aux gas heater temperature, 400°C ; sheath gas, 40; auxiliary gas, 13; spray voltage, 3.5 kV for positive mode and negative mode. The capillary temperature was set at 350°C , and the S-lens was set at 55°C . (2) A DDA method was built as follows: full-scan range: 60 to 900 (m/z); resolution for MS1 and ddMS2: 70,000 and 17,500, respectively; maximum injection time (IT) for MS1 and ddMS2: 100 ms and 45 ms; automatic gain control (AGC) for MS1 and ddMS2: $3 \text{ E} + 6$ and $2 \text{ E} + 5$; isolation window: 1.6 m/z; normalized collision energies (NCEs): 10, 17, 25 or 30, 40, 50. (3) A full-scan method was built as follows: full-scan range: 60 to 900 (m/z); resolution: 140,000; maximum injection time: 100 ms; AGC: $3 \text{ E} + 6$ ions.

Compound Annotation and Quantification—The raw files were submitted to Thermo Compound Discover 2.1 and processed with an untargeted metabolomics workflow with minor modification to find and identify the differences between samples.

Subsequently, retention time alignment, unknown compound detection, and compound grouping across all samples were performed. Then, the elemental compositions for all compounds were predicted, file gaps and chemical background across all samples were hidden by using blank samples. mzCloud and ChemSpider were used to identify the compounds. Compounds mapped to biological pathways were analyzed using the KEGG database. For retention time alignment, the maximum time shift was 2 min, and a tolerance of 0.5 min was used for grouping unknown compounds. Mass tolerance was set as 10 ppm for feature detection and 5 ppm for compound annotation. The exact mass of each feature was submitted to ChemSpider with four databases selected (BioCyc; Human Metabolome Database; KEGG; LipidMAPS). The intensity of each mass ion was normalized with respect to the total ion count to generate a data matrix that included the retention time, m/z value, and normalized peak area.

Multivariate Pattern Recognition Analysis—The relative intensity data of annotated metabolites were employed as explanatory variables and then subjected to multivariate pattern recognition analysis using the SIMCA 13.0 software package (Umetrics, Umea, Sweden). Supervised orthogonal partial least squares–discriminant analysis (OPLS-DA) was performed for class discrimination and biomarker identification (11).

OPLS-DA provided the most complete representation of the data, which were visualized using the first principal component (p[1]) and the orthogonal component (o[1]). As mentioned in the literature, OPLS-DA revealed differences of different groups, which were necessary to eliminate outliers and enhance the quality of the model (12, 13). Moreover, two parameters were calculated. $R^2\text{X}$ and $R^2\text{Y}$ show an explained variance in the matrix of data and class membership, respectively, and Q^2 is the predictive capability of the model, which is commonly used to indicate the quality of the model. An excellent model always has the values of $R^2\text{Y}$ and Q^2 , which are close to 1.0 (14). Then, a permutation test was also performed to evaluate the robustness of the OPLS-DA model.

LC-MS Analysis for Proteomics—The experimental system was designed for 10-plex tandem mass tag (TMT)-based mass spectrometry analysis. We analyzed ten samples, which were two

biological replicates for each NPRA knockout mouse and the matched littermate.

Sample Preparation—One-hundred milligrams of tissue in a 1.5 ml EP tube was lysed in 1000 μl buffer consisting of RIPA protease inhibitor cocktail and 1 mM PMSF. Protein quantification was performed using a bicinchoninic acid (BCA) assay kit. Then, 100 μg protein from each sample was precipitated with an acetone precipitation method. Furthermore, resuspended protein was used for tryptic digestion, TMT labeling, SDC cleaning, and peptide desalting for base-reversed-phase (RP) fractionation.

Quantitative Proteomics by Multiplexed TMT-MS—For proteomic analysis of cardiac tissues, after protein recovery, samples were extracted, digested with trypsin, and labeled with TMT reagents. NPRA knockout samples were labeled with 126 C-tag, 127 N-tag, 127 C-tag, 128 N-tag, and 128 C-tag, whereas the control was labeled with 129 N-tag, 129 C-tag, 130 N-tag, 130 C-tag, and 131 N-tag. Labeled samples were mixed in equal amounts, desalted using C18 spin tips, and freeze-dried. The pooled peptides were separated into peptides, fractionated into 120 fractions with high pH RPRP-HPLC, and then combined into eight fractions using a C18 column (Waters BEH C18 2.1 \times 150 mm, 5 μm). For each fraction, $\sim 2 \mu\text{g}$ peptide was separated and analyzed with a nano-UPLC (EASY-nLC1200) coupled to a Q-Exactive mass spectrometer (Thermo Finnigan). Separation was performed using a reversed-phase column (100 μm , ID \times 15 cm, Reprosil-Pur 120 C18-AQ, 1.9 μm , Dr Math). The mobile phases were H₂O with 0.1% FA, 2% ACN (phase A) and 80% ACN, 0.1% FA (phase B). Separation of the sample was executed with a 90 min gradient at a 300 nl/min flow rate. The gradient was as follows: 8–30% for 70 min, 30–40% for 12 min, 40–100% for 2 min, 100% for 2 min, 100–2% for 2 min, and 2% for 2 min. Data-dependent acquisition was performed in profile and positive mode with an Orbitrap analyzer at a resolution of 70,000 (@200 m/z) and m/z range of 350–1600 for MS1. For MS2, the resolution was set to 35,000 with a fixed first mass of 110 m/z. The AGC target for MS1 was set to $3.0 \text{ E} + 6$ with a max IT of 50 ms, and that for MS2 was set to $1.0 \text{ E} + 5$ with a maximum IT of 45 ms. The top 20 most intense ions were fragmented by high-energy collision dissociation (HCD) with an NCE of 32% and an isolation window of 2 m/z. The dynamic exclusion time window was 30 s.

Multivariate Pattern Recognition Analysis—Principal component analysis (PCA) was performed to study the overall protein expression pattern between the NPRA^{-/-} mice and NPRA^{+/+} mice.

MaxQuant Database Search—Raw MS files were processed with MaxQuant (Version 1.5.6.0). The protein sequence database (UniProt_organism_2016_09) was downloaded from UniProt. Species of sequence database is from Musculus (mouse) (strain: C57BL/6J) sequence database. This database and its reverse decoy were then searched against MaxQuant software. Number of entries in the database actually searched is 55,474 proteins. Mass tolerance for precursor ions and mass tolerance for fragment ions both are 10 ppm. The quantification type was reporter ion MS2 with n-plex TMT specific to Lys (K) and an unmodified N-term; trypsin was set as a specific enzyme with up to three mismatches; oxidation [M] and acetyl [protein N-term] were considered as variable modifications (max number of modifications per peptide is 3), carbamidomethyl [C] was set as fixed modification; both the peptide and protein false discovery rates (FDRs) should be less than 0.01. Only unmodified unique peptides were used for quantification. All the other parameters were reserved as default. For quantitative analysis, only proteins with at least one unique peptide match with TMT ratios were considered. A ≥ 1.20 - or ≤ 0.83 -fold cutoff value was used to identify upregulated and downregulated proteins, respectively, with a *p*-value of <0.05 .

Gene Ontology (GO) Enrichment—The GO project is a major bioinformatics initiative to unify the representation of gene and gene product attributes across all species. It provides an ontology of

defined terms representing gene product properties. To probe the main biological process (BPs), cellular components (CCs), and molecular functions (MFs) of differentially abundant proteins, the responsive proteins were further summarized based on GO terms. In this study, functional annotation and classification of all identified proteins were performed using the Blast2GO program (15) against the nonredundant NCBI protein database.

KEGG Enrichment—The KEGG database (16) is a collection of manually drawn KEGG pathway maps representing experimental knowledge on metabolism and various other functions of the cell and organism. Furthermore, the KEGG map module was employed to display the enzymatic functions of the detected proteins from the perspective of the metabolic pathways in which they participate. In this study, we analyzed differentially abundant proteins-associated metabolic pathways to elucidate the effects of NPRA knockout on the metabolic phenotype of cardiovascular disease by KEGG enrichment.

STRINGdb Protein–Protein Interaction (PPI) Analysis—STRING (<http://string-db.org/>) is a database of known and predicted PPIs. The interactions include direct (physical) and indirect (functional) associations. They stem from computational prediction, knowledge transfer between organisms, and interactions aggregated from other (primary) databases. The minimum required interaction score was set as 0.400.

Statistic Rationale—Multivariate statistical analysis was performed using the SIMCA 13.0 software package (Umetrics, Umeå, Sweden). OPLS-DA was used to study an overview of the change in metabolic pattern between NPRA^{-/-} mice and NPRA^{+/+} mice, and the overall protein expression pattern between the groups was further investigated by PCA. The statistical analyses were performed by SPSS software (version 18.0). Data are presented as the mean ± standard error of the mean (SEM). An independent sample *t*-test was applied to compare metabolite levels and protein levels between two groups. A value of *p* < 0.05 was considered statistically significant. Metabolic pathway analysis was performed on the basis of the KEGG database.

RESULTS

NPRA-Deficient Mice Have Distinct Metabolic Patterns Compared With Control Mice

It is reported that NPRA-deficient mice have low mRNA and protein expression (17, 18). Our previous study (9) also confirmed that the expression in mRNA and protein of NPRA decreased in the cardiac tissues of the mice.

To visualize the metabolic profiles of plasma and cardiac tissues, OPLS-DA was performed based on the LC/MS spectra of the mice with myocardial-specific knockout of NPRA and the matched littermates. We found that NPRA-deficient mice displayed a peculiar metabolic phenotype relative to their controls in both the heart tissue and plasma (Fig. 1, A and C), and an OPLS-DA model overview analysis for the heart (Fig. 1B) and plasma (Fig. 1D) fully revealed that the distinct metabolic pattern along the direction of P [1] is very significant. However, we were astonished by the result that NPRA-deficient mice and their controls had no clear changes in the heart structure and function or heart-to-body weight ratio (supplemental Fig. S1).

NPRA Deficiency Causes Metabolic Changes in Mice

The detailed metabolic changes are illustrated in the cluster thermal chart for plasma (Fig. 2A) and heart (Fig. 2B). In total,

33 metabolites were identified in cardiac tissues and 54 in plasma (supplemental Excels S1 and S2). Compared with the matched littermates, the NPRA-deficient mice had 20 upregulated and six downregulated metabolites in tissues as well as 25 upregulated and 23 downregulated metabolites in plasma. In addition, plasma and cardiac tissue metabolites that significantly altered between the NPRA-deficient mice and the matched littermates were highlighted in the volcano plot (Fig. 2, C and D), respectively. The plasma levels of phosphocreatine (PCr) in NPRA-deficient mice were significantly decreased compared with the levels in the matched littermates, and the levels of urochloralic acid decreased significantly. For cardiac tissues, the levels of uridine monophosphate (UMP), adenosine 5'-monophosphate (AMP), formiminoglutamic acid (FIGLU), and lactobionic acid were markedly increased, and carginic acid was significantly decreased in the NPRA-deficient mice. Together, NPRA deficiency resulted in an increase in nucleotide biosynthesis and histidine metabolism in the heart tissues. However, decreased creatine metabolism was observed in the plasma, and other metabolic disorders were shown in both the cardiac tissue and plasma.

Changed Proteins Probably Associated With Metabolic Processes Were Identified in Cardiac-Specific NPRA-Deficient Mice

To gain a global view of the mechanism of DEPs, we analyzed the results of a TMT-based mass spectrometry quantitative proteomics study for biological replicates of NPRA-deficient mice and matched littermates (Fig. 3A). A total of 12,768 peptides and 2454 proteins were detected. A total of 2302 proteins were quantified from each sample (1% FDR). Proteins with fewer than two unique peptides were excluded, and the resulting 136 differentially abundant proteins (supplemental Excel S3) were used for further analysis. A hierarchical cluster heat map (Fig. 3B) shows changes in relative protein abundances across NPRA-deficient mice and their matched littermates. Furthermore, PCA (Fig. 3C) was applied to investigate the protein expression patterns. The data illustrated the clear discrimination of protein expression patterns of the cardiac tissues between the two groups. Among the differentially abundant proteins, 54 proteins showed higher expression and 82 showed lower expression in NPRA-deficient mice than in controls, and we found that proteins including palmitoyl-protein thioesterase 1 (Ppt1), lactate dehydrogenase D (Ldhd), cathepsin D (Ctsd), Lghd2b, Fah, muscle assembly regulating factor titin-cap (Tcap), Neb, neurotrophic tyrosine kinase, receptor, type 3 (Ntrk3), myosin Heavy Chain 7 (Myh7), and 3-hydroxybutyrate dehydrogenase type 1 (Bdh1) significantly increased, whereas proteins including ribosomal Protein L36 (Rpl36), ATP synthase, H⁺ transporting, mitochondrial Fo complex subunit F2 (ATP5J2), ribosomal protein L36A-like (Rpl36a), transferrin receptor (Tfrc), Qki, Mrps21 (mitochondrial ribosomal protein S21),

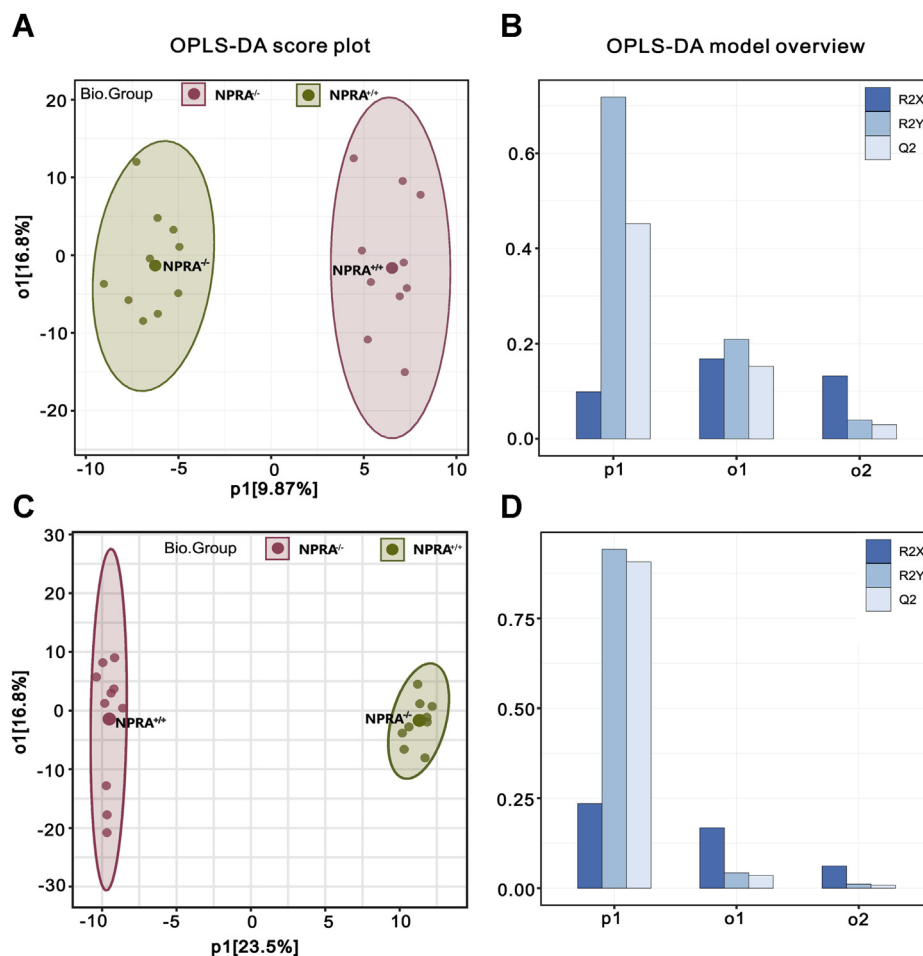


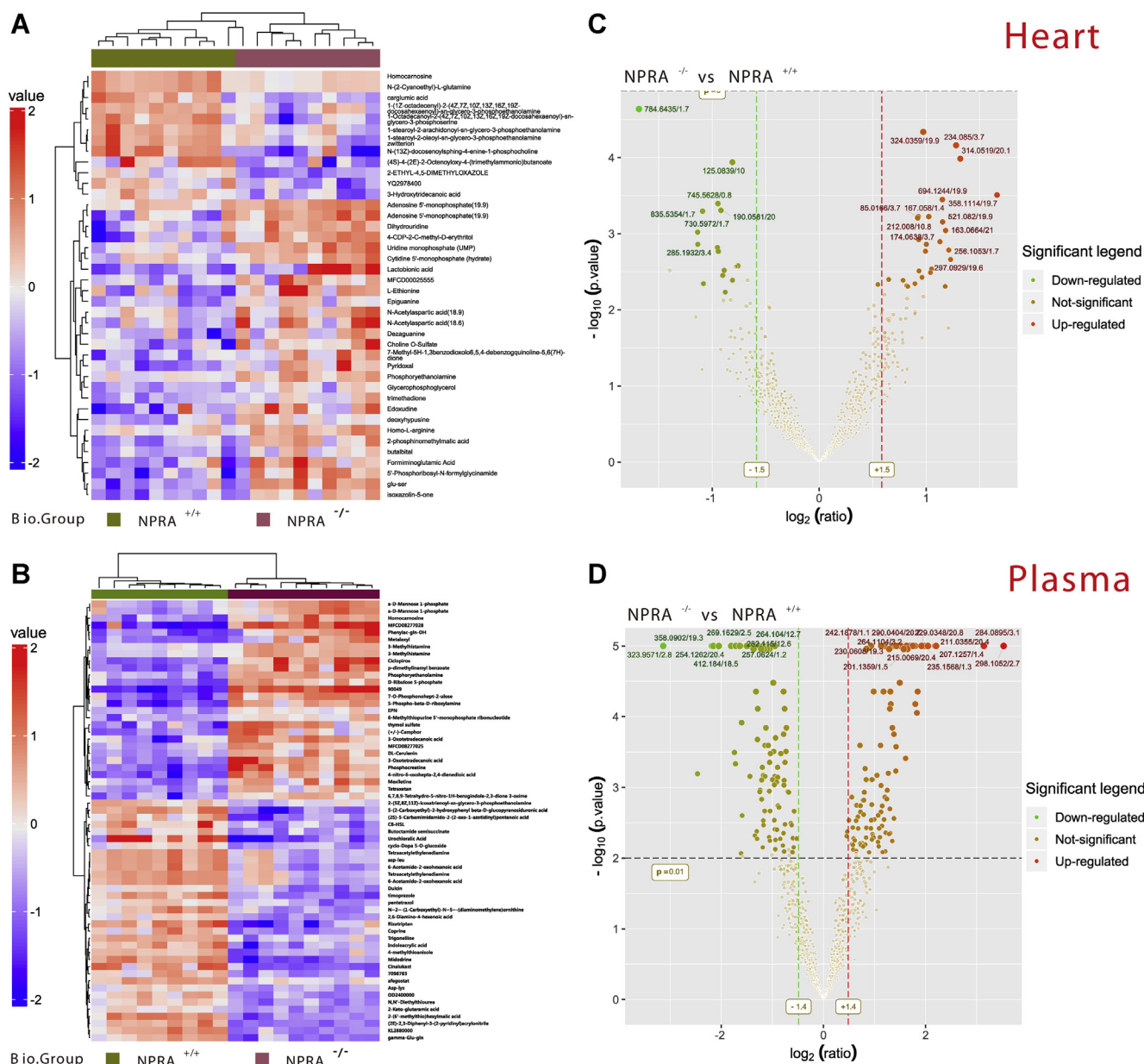
FIG. 1. **Pattern recognition analysis of cardiac samples and plasma samples.** A and C, PLS-DA for the models discriminating the NPRA-deficient mice (purple dots) and wild-type mice (green dots) in the heart and plasma. p[1] represents the first principal component, and o[1] represents the orthogonal component. B and D, an OPLS-DA model overview analysis. R²X and R²Y show an explained variance in the matrix of data and class membership, respectively, and the Q², predictive capability of the model.

Myl6(myosin light polypeptide 6), Fibulin 5 (Fbln5), and Family with sequence similarity136, member A, (Fam136 A) significantly decreased (Fig. 3D).

GO Analysis and KEGG Pathway Analysis of Proteins Induced by Specific Knockout of NPRA

The differentially abundant proteins identified in NPRA-deficient mice versus control mice were further categorized using GO annotation. The responsive proteins were classified based on GO terms: BPs, CCs, and MFs. The differentially abundant proteins corresponded to 80, 53, and 23 terms for BPs, CCs, and MFs, respectively. The top ten altered GO terms in the NPRA-deficient group classified by BP, MF, and CC are shown in Figure 4A (supplemental Excel S4). According to the percentage of genes (>40%) in GO enrichment, the BP analysis revealed that most of the proteins with altered expression belong to two major processes. Nucleoside triphosphate metabolic processes mainly include purine

nucleoside triphosphate metabolic processes and cardiac muscle contraction functions including actin-mediated cell contraction, actin-filament-based movement, cardiac muscle tissue morphogenesis, cell communication involved in cardiac conduction, and regulation of the action potential of ventricular cardiac muscle cells. The CC analysis indicated that these proteins were mainly located in the mitochondria and ribosome and were integral components of the membrane or part of the mitochondrial, ribosome, and respiratory chain complex, whereas molecular function analysis showed that the identified proteins were mainly involved in purine deoxyribonucleotide binding, electron transfer activity, and cardiac muscle cell action potential. In accordance with this, NPRA deficiency with increased AMP, UMP, and D-ribulose 5-phosphate metabolism indicated that nucleotide biosynthesis was changed. Simultaneously, we found that cytochrome c oxidase subunit 7c (Cox7c), cytochrome c oxidase subunit 7b, (Cox7b), ATP5J2, ubiquinol-cytochrome c



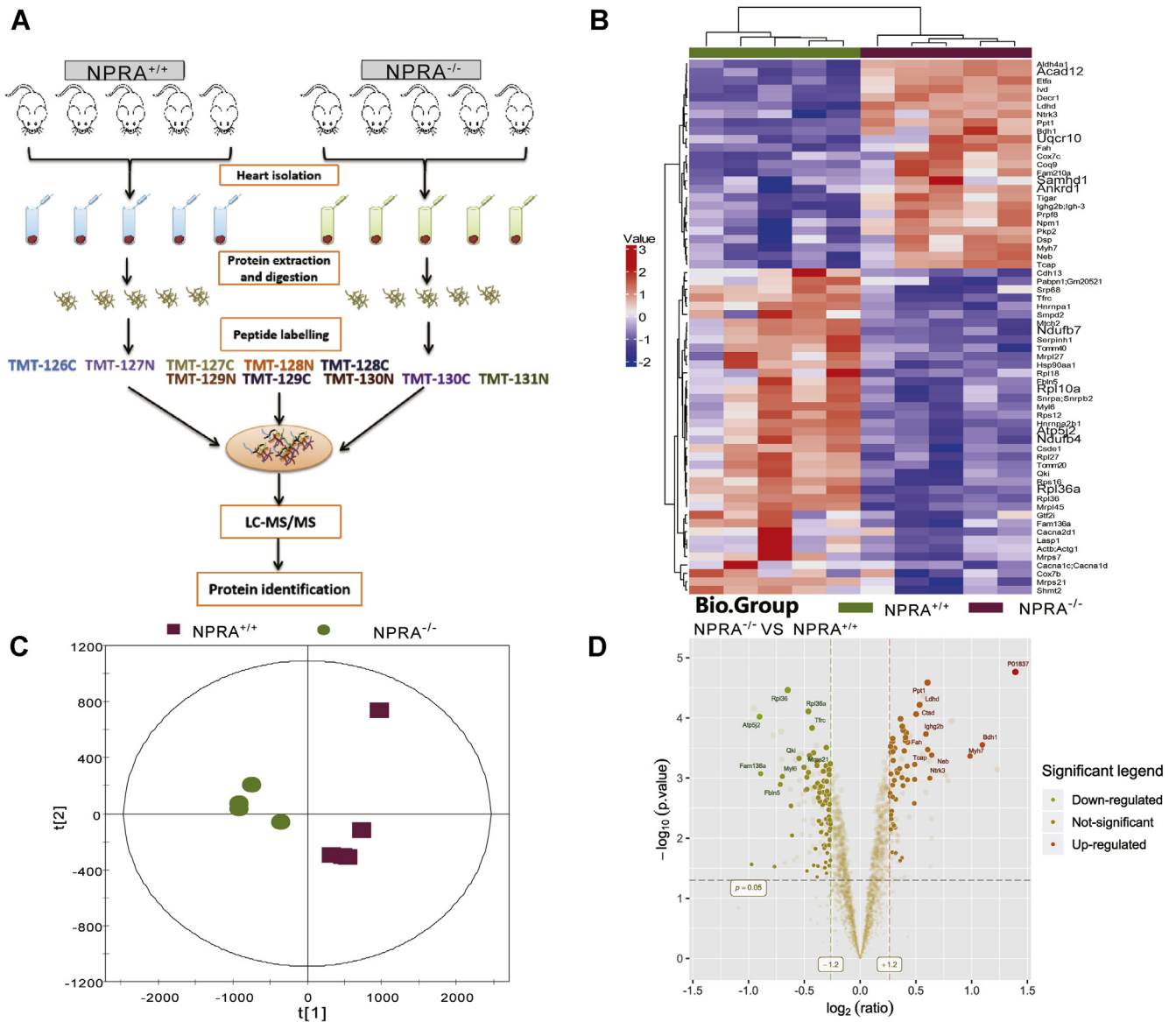


FIG. 3. Differentially abundant proteins in the mouse myocardium ($0.83 < \text{fold change} < 1.2$, and $p\text{-value} < 0.05$). A, experimental designs to investigate the mechanism of NPRA deficiency in mice with TMT-based quantitative proteomic analysis. B, hierarchical clustering analysis of proteins that were differentially expressed in the hearts between NPRA-deficient mice (green box) and the matched littermates as a control (purple box). Each group contains five individuals. Blue indicates lower expression, and red indicates high expression. C, the PCA scatter plot was used to evaluate the changing expression profiles of proteins between NPRA-deficient mice (green box) and the control tissue samples (purple box). D, the differentially abundant proteins (shown in red font) with statistical significance from cardiac tissues between NPRA-deficient mice and the controls screened using a volcano plot. The vertical line represents a boundary of the differentially abundant proteins and other proteins, and the horizontal line corresponds to a p -value equal to 0.05.

PPI Networks

PPI network analysis displayed a close interaction among the differentially abundant proteins that corresponded to GO terms and KEGG pathways with the lowest p -value. The differentially abundant proteins showed mutual interactions in this complex PPI network (Fig. 5). This network may provide insight into the potential interactions between protein candidates and their target proteins.

DISCUSSION

It is well known that ANP/BNP-NPRA signals play a very important role in cardiovascular activity. In the current study, we proved that deterioration of NP signaling results in metabolic dysfunction involving a protein-metabolite interaction pathway. This point of view is based on the following findings: (1) in mice with myocardial-specific NPRA knockout, metabolic functions were aberrant. (2) Concurrently, the expression

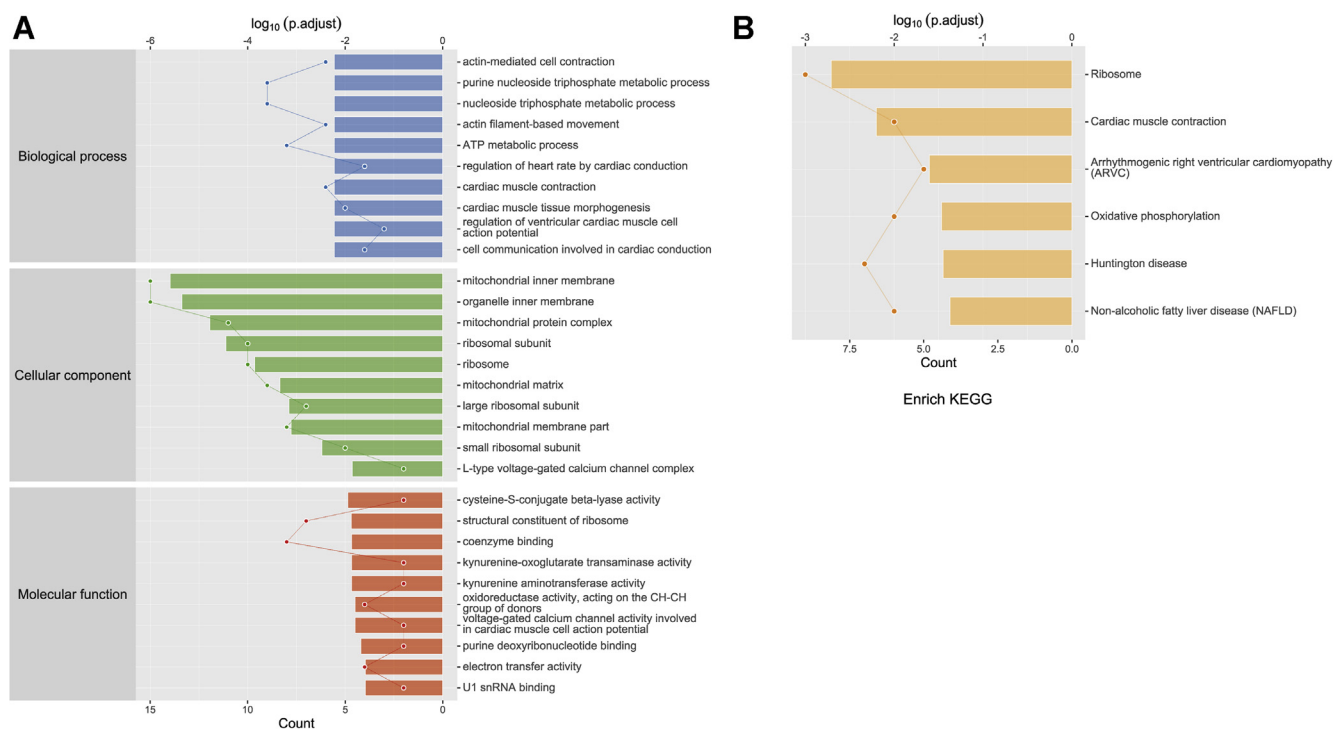


FIG. 4. GO and KEGG pathway analyses of differentially abundant proteins. A, enriched GO terms, top axis is \log_{10} (adjusted p -value), bottom axis is the gene count. The top ten changed GO terms associated with BPs, CCs, and MFs were ranked by fold enrichment and enrichment score. B, KEGG pathway analysis of differentially abundant proteins involved in metabolic pathways. Enriched KEGG terms, if no protein matched or less than five enriched items were found, are displayed on the plot. The top axis is \log_{10} (adjusted p -value), and the bottom axis is the gene count.

profiles of proteins and peptides were different between the NPRA-deficient and wild-type mice. (3) A protein–metabolite interaction pathway involved in cardiac metabolism was constructed by the means of GO analysis and KEGG pathway analysis.

NPs are a group of peptide hormones mainly secreted from the heart and are involved in signaling *via* cGMP-coupled receptors. NPs are well known for their renal and cardiovascular actions, reducing arterial blood pressure as well as sodium reabsorption. Novel metabolic functions have been discovered in recent years, including activation of lipolysis, lipid oxidation, and mitochondrial respiration (19). Despite high circulating concentrations of immunoreactive peptides, functional NP deficiency has been observed in type 2 diabetes mellitus and cardiometabolic complications, pointing to an involvement of blunt NP signaling in the pathophysiology of metabolic disorders (20). Currently, the cardiometabolic changes after NPRA knockout indicate the regulatory roles of the NP system on the metabolism of the myocardium.



Previous reports have demonstrated that NPRA deficiency causes an increased heart weight/weight ratio and cardiac hypertrophy in mice, which increases sensitivity to heart failure and obesity (3, 21, 22). In the current study, it was unexpected that no significant morphological change was detected, and the heart weight/weight ratio was unchanged. However, in the

proteomic analysis, we found increased expression of β -myosin heavy chain (MHC) 7 (Myh7). Many researchers (23–25) have demonstrated that Myh7 is closely associated with myocardial hypertrophy. It is the dominant pathogenic gene that harbours mutations in 20–30% of cases of familial hypertrophic cardiomyopathy (HCM) (26). We speculated that it may be under the stimulation of other diseases; the above pathological changes caused by NPRA knockout will be clearer or because the mice are more tolerant to NPRA knockout and have a certain compensatory response, so they have not shown a strong pathological response.




Recently, studies have suggested that metabolic reprogramming participates in the onset and progression of cardiovascular diseases. In this study, NPRA deficiency resulted in an increase in nucleotide biosynthesis and histidine metabolism in heart tissues. UMP is essential for cell proliferation (27), and AMP is defined as an energy metabolism-related metabolite (28) that participates in nucleotide biosynthesis. We found that UMP and AMP are both increased in the heart tissues of NPRA-deficient mice. As reported, phosphocreatine (PCr) plays an important role in the energy metabolism of the heart, and a decrease in its intracellular concentration results in alteration of myocardium energetics and work (29). In some diseases, such as myocardial infarction, viral myocarditis, dermatomyositis, muscular dystrophy, pericarditis, and

Proteins: 55
Interactions: 110
Expected interactions: 39




Known Interactions

-  From curated databases
-  Experimentally determined

Predicted Interactions

-  Gene neighborhood
-  Gene fusions
-  Gene co-occurrence

Others

-  Textmining
-  Co-occurrence
-  Protein homology

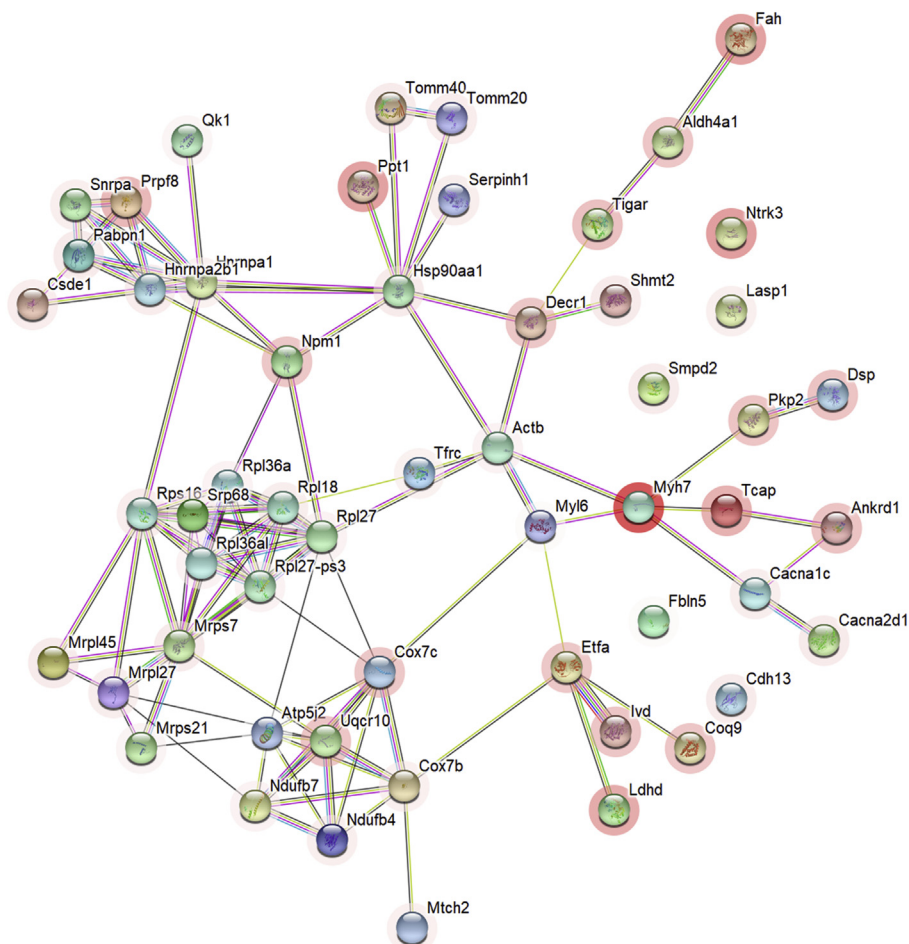


FIG. 5. A functional protein association network was generated using STRING 11.0. The line thickness indicates the strength of data support.

cerebrovascular accidents, creatine kinase can contribute to a pathological increase and can convert creatine to PCr (30, 31). A large number of studies have confirmed that PCr can improve cardiac energy metabolism; preserve cardiac excitability, conductivity, and contractility; reduce the incidence of arrhythmia; and protect cardiac function, and PCr is now widely used for extracorporeal circulation, coronary heart disease, heart failure, and myocardial infarction (32–35). In this study, we found that PCr significantly decreased in the plasma of NPRA-deficient mice. This result indicated that the loss of NPRA leads to changes in the homeostasis of cardiac energy metabolism. We hypothesized that it may be involved in the effect of creatine kinase. In addition, 2-keto-glutaramic acid (α -KG) is an endogenous intermediary metabolite in the tricarboxylic acid cycle (TCA), and it acts as an energy donor, an amino acid biosynthesis precursor, a signaling molecule, and a regulator of epigenetic processes and cellular signaling via protein binding in multiple metabolic and cellular pathways (36, 37). However, the level of α -KG in NPRA-deficient mice increased abnormally. As depicted above, the NPRA-deficient

mice showed energy metabolism disorders. N-acetyl-L-aspartic acid (NAA) is the N-acetylated derivative of the amino acid L-aspartate (ASP), present in the central nervous system (CNS) of humans and other animals (38). Interestingly, an increased level of NAA in the myocardial tissues of NPRA-deficient mice was detected. L-Histidine is one of the 20 standard proteinogenic amino acids present in the proteins of all living organisms. Histidine biosynthesis is an unbranched pathway with ten enzymatic reactions, starting with phosphoribosyl pyrophosphate (PRPP) and leading to L-histidine. It is considered an essential amino acid for humans, and its degradation can produce N-formiminoglutamate (FIGLU) and glutamate (39). We found that FIGLU increased in the cardiac tissues of NPRA-deficient mice. In summary, the NPRA-deficient mice had a special biosynthetic process to satisfy the energy supply during their growth.

As described, all these results demonstrated the different holistic metabolic pathways in the cardiac tissues of NPRA-deficient mice and controls. Mice with NPRA deficiency have a disordered metabolism in both cardiac tissues and plasma.

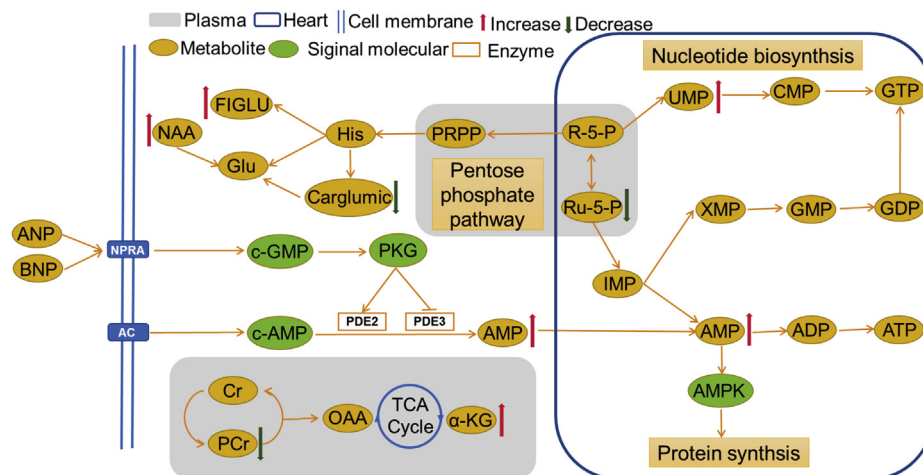


FIG. 6. Disturbed metabolic pathways in heart tissues and plasma of NPRA-deficient mice and wild type mice. α -KG, α -ketoglutarate; ADP, adenosine diphosphate; AMP, adenosine 5'-monophosphate; ATP, adenosine triphosphate; CMP, cytosine monophosphate; Cr, creatine; FIGLU, formiminoglutamic acid; GDP, guanine diphosphate; Glu, glutamate; GTP, guanine triphosphate; His, histidine; IMP, inosine monophosphate; NAA, N-acetyl aspartate; OAA, oxaloacetate; PCr, phosphocreatine; Carglumic; PRPP, 5-phosphoribosyl 1-pyrophosphate; R-5-P, D-ribulose-5-phosphate; Ru-5-P, UMP, uridine monophosphate.

In the cardiac tissues, the NPRA signal is involved in nucleotide biosynthesis and histidine metabolism, while in the plasma, the NPRA signal mainly participates in the TCA cycle and pentose phosphate pathway (Fig. 6).

In addition, cytochrome c oxidase (COX) is the terminal enzyme of the electron transport chain and catalyzes the transfer of electrons from cytochrome c to oxygen. It is composed of three largest subunits (COX I, II, and III) encoded by mitochondrial DNA and 11 subunits (COXIV, Va, Vb, VIa, VIb, VIc, VIIa, VIIb, VIIc, VIII, and NDUFA4) encoded by nuclear DNA (40, 41). In this study, we found that COX VIIb decreased but COX VIIc increased in NPRA-deficient mice by proteomic analysis. Furthermore, we found that the level of subunit Uqcrl0 of complex III also increased. Additionally, proteomic data showed that ATP5J2 (mitochondrial membrane ATP synthase) decreased significantly. It is a key enzyme involved in energy metabolism, and it catalyzes the synthesis of ATP from substrates to provide cells with the energy required to perform various life activities (nerve conduction, muscle contraction, material transport, etc.) (42). Given the critical role of COX in regulating oxygen consumption and ATP production, we speculate that NPRA may play an important role in myocardial energy metabolism by regulating the role of cox and then affecting myocardial mitochondrial function. In general, we first reported that NPRA deficiency may contribute to myocardial mitochondrial dysfunction. The data echo the metabolic results and confirm the metabolic changes.

In conclusion, NP signaling plays important roles in the regulation of cardiac metabolism. In the present study, we first demonstrated the holistic metabolic patterns of cardiac tissue in NPRA-deficient mice. The data suggest that abnormalities in NPRA may be implicated in various metabolic disorders and the changes in protein expression. The underlying mechanism

is involved in the protein–metabolite interaction pathway. This finding provides valuable clues for possible novel pathways that are regulated by downstream signals of NPRA and modulate cardiac metabolism. The components involved in the functional roles of this network may serve as potential therapeutic targets for cardiac metabolic disorders and are worthy of further investigation.

To our knowledge, this was the first attempt to explore the metabolic disturbances in NPRA-deficient mice by LC/MS-based metabolomic techniques and proteomic techniques. We found that NPRA-deficient mice exhibit extreme metabolic disorders, but further proteomic analysis revealed that the protein expression levels involved in the metabolic processes actually changed. Unfortunately, we have not verified the mechanisms of the specific roles of related differential proteins in NPRA knockout-induced metabolic disorders. The metabolic data and proteomic data complemented each other and fully displayed the significant effects of NP signaling on the myocardium and systemic circulation.

DATA AVAILABILITY

All data are shown in supplementary materials. The mass spectrometry proteomics data have been deposited to the ProteomeXchange Consortium via the PRIDE (43) partner repository with the data set identifier PXD020997.

Supplemental data—This article contains [supplemental data](#).

Acknowledgments—The present study was completed successfully with the help of Dr Jin-Song Chen for his valuable suggestions for this study.

Funding and additional information—This work is supported by the National Natural Science Foundation of China (Grant No. 81870172), the Shaanxi Provincial Key Research and Development Project (2018ZDXM-SF-068 and 20YXYJ003(3)), and Annual Project (2020QN007) of Xi'an International Medical Center Hospital, Shaanxi Province.

Author contributions—P. C., Y. N., and X. Z. contributed to experimental studies, data analysis, and article writing. J. Z., X. W., and X. S. played a major role in organizing animal experiments. B. C. and J. Y. contributed to financial support and gave final approval for the publication of the article.

Conflict of interest—The authors declare no competing interests.

Abbreviations—The abbreviations used are: ACN, acetonitrile; GC-A, guanylyl cyclase-A; GC-MS, gas chromatography-mass spectrometry; LC-MS, liquid chromatography-mass spectrometry; LVEF, left ventricular ejection fraction; LVFS, left ventricular fractional shortening; MeOH, methanol; NMR, nuclear magnetic resonance; NPs, natriuretic peptides; o[1], the orthogonal component; OPLS-DA, supervised orthogonal partial least squares-discriminant analysis; p[1], the first principal component; PCA, principal component analysis; PVDF, polyvinylidene difluoride; TMT, tandem mass tag.

Received August 24, 2020, and in revised form, February 12, 2021
Published, MCPRO Papers in Press, March 31, 2021, <https://doi.org/10.1016/j.mcpro.2021.100072>

REFERENCES

- Fu, S., Ping, P., Wang, F., and Luo, L. (2018) Synthesis, secretion, function, metabolism and application of natriuretic peptides in heart failure. *J. Biol. Eng.* **12**, 2
- Potter, L. R. (2011) Natriuretic peptide metabolism, clearance and degradation. *Febs J.* **11**, 1808–1817
- Gupta, D. K., and Wang, T. J. (2015) Natriuretic peptides and cardiometabolic Health. *Circ. J.* **8**, 1647–1655
- Cannone, V., Cabassi, A., Volpi, R., and Burnett, J. C. (2019) Atrial natriuretic peptide: A molecular target of novel therapeutic approaches to Cardio-metabolic disease. *Int. J. Mol. Sci.* **13**, 3265
- Zhao, H., Du, H., Liu, M., Gao, S., Li, N., Chao, Y., Li, R., Chen, W., Lou, Z., and Dong, X. (2018) Integrative proteomics-metabolomics strategy for pathological mechanism of Vascular Depression mouse model. *J. Proteome Res.* **17**, 656–669
- Wei, T., Zhao, L., Jia, J., Xia, H., Du, Y., Lin, Q., Lin, X., Ye, X., Yan, Z., and Gao, H. (2015) Metabonomic analysis of potential biomarkers and drug targets involved in diabetic nephropathy mice. *Sci. Rep.* **5**, 11998
- Wishart, D. S. (2016) Emerging applications of metabolomics in drug discovery and precision medicine. *Nat. Rev. Drug Discov.* **7**, 473–484
- Zhao, C., Han, S., Yang, S., and Xin, W. (2019) Validation and application of a novel LC/MS/MS method for the determination of isoginkgetin in rat plasma. *Biomed. Chromatogr.* **11**, e4667
- Chen, B., Chang, P., Shen, X., Zhang, X., Zhang, J., Wang, X., and Yu, J. (2021) Cardiac-specific deletion of natriuretic peptide receptor A induces differential myocardial expression of circular RNA and mRNA molecules involved in metabolism in mice. *Mol. Med. Rep.* **1**, 50
- Yu, J., Bulk, E., Ji, P., Hascher, A., Tang, M., Metzger, R., Marra, A., Serve, H., Berdel, W. E., Wiewroth, R., Koschmieder, S., and Müller-Tidow, C. (2010) The EPHB6 receptor tyrosine kinase is a metastasis suppressor that is frequently silenced by promoter DNA hypermethylation in non-small cell lung cancer. *Clin. Cancer Res.* **8**, 2275–2283
- Yang, M., Li, X., Li, Z., Ou, Z., Liu, M., Liu, S., Li, X., and Yang, S. (2013) Gene features selection for three-class disease classification via multiple orthogonal partial least square discriminant analysis and S-plot using microarray data. *PLoS One* **12**, e84253
- Boccard, J., and Rutledge, D. N. (2013) A consensus orthogonal partial least squares discriminant analysis (OPLS-DA) strategy for multiblock Omics data fusion. *Anal. Chim. Acta* **769**, 30–39
- Yang, Q., Lin, S., Yang, J., Tang, L., and Yu, R. (2017) Detection of inborn errors of metabolism utilizing gc-ms urinary metabolomics coupled with a modified orthogonal partial least squares discriminant analysis. *Talanta* **165**, 545–552
- Dong, F., Deng, D., Chen, H., Cheng, W., Li, Q., Luo, R., and Ding, S. (2015) Serum metabolomics study of polycystic ovary syndrome based on UPLC-QTOF-MS coupled with a pattern recognition approach. *Anal. Bioanal. Chem.* **16**, 4683–4695
- Park, T. J., Park, J. H., Lee, G. S., Lee, J. Y., Shin, J. H., Kim, M. W., Kim, Y. S., Kim, J. Y., Oh, K. J., Han, B. S., Kim, W. K., Ahn, Y., Moon, J. H., Song, J., Bae, K. H., et al. (2019) Quantitative proteomic analyses reveal that GPX4 downregulation during myocardial infarction contributes to ferroptosis in cardiomyocytes. *Cell Death Dis.* **11**, 835
- Dong, Z., Chen, Z., Wang, H., Tian, K., Jin, P., Liu, X., Mchunu, N. P., Permaul, K., Singh, S., and Niu, D. (2017) Tandem mass tag-based quantitative proteomics analyses reveal the response of *Bacillus licheniformis* to high growth temperatures. *Ann. Microbiol.* **67**, 501–510
- Oliver, P. M., Fox, J. E., Kim, R., Rockman, H. A., Kim, H. S., Reddick, R. L., Pandey, K. N., Milgram, S. L., Smithies, O., and Maeda, N. (1997) Hypertension, cardiac hypertrophy, and sudden death in mice lacking natriuretic peptide receptor A. *Proc. Natl. Acad. Sci. U. S. A.* **26**, 14730–14735
- Pandey, K. N. (2019) Genetic Ablation and guanylyl cyclase/natriuretic peptide receptor-A: Impact on the pathophysiology of cardiovascular dysfunction. *Int. J. Mol. Sci.* **16**, 3946
- Vellaichamy, E., Sommana, N. K., and Pandey, K. N. (2005) Reduced cGMP signaling activates NF-kappaB in hypertrophied hearts of mice lacking natriuretic peptide receptor-A. *Biochem. Biophys. Res. Commun.* **1**, 106–111
- Zois, N. E., Bartels, E. D., Hunter, I., Kousholt, B. S., Olsen, L. H., and Goetze, J. P. (2014) Natriuretic peptides in cardiometabolic regulation and disease. *Nat. Rev. Cardiol.* **7**, 403–412
- Gardner, D. G., Chen, S., Glenn, D. J., and Grigsby, C. L. (2007) Molecular biology of the natriuretic peptide system: Implications for physiology and hypertension. *Hypertension* **3**, 419–426
- Vellaichamy, E., Zhao, D., Somanna, N., and Pandey, K. N. (2007) Genetic disruption of guanylyl cyclase/natriuretic peptide receptor-A upregulates ACE and AT1 receptor gene expression and signaling: Role in cardiac hypertrophy. *Physiol. Genomics* **2**, 193–202
- Montag, J., Kowalski, K., Makul, M., Ernstberger, P., Radocaj, A., Beck, J., Becker, E., Tripathi, S., Keyser, B., Mühlfeld, C., Wissel, K., Pich, A., van der Velden, J., Dos Remedios, C. G., Perrot, A., et al. (2018) Burst-like Transcription of mutant and Wildtype MYH7-Alleles as possible Origin of cell-to-cell contractile imbalance in hypertrophic cardiomyopathy. *Front. Physiol.* **9**, 359
- Montag, J., Syring, M., Rose, J., Weber, A. L., Ernstberger, P., Mayer, A. K., Becker, E., Keyser, B., Dos Remedios, C., Perrot, A., van der Velden, J., Francino, A., Navarro-Lopez, F., Ho, C. Y., Brenner, B., et al. (2017) Intrinsic MYH7 expression regulation contributes to tissue level allelic imbalance in hypertrophic cardiomyopathy. *J. Muscle Res. Cell Motil.* **3**, 291–302
- Wang, J., Wan, K., Sun, J., Li, W., Liu, H., and Han, Y. (2018) Phenotypic diversity identified by cardiac magnetic resonance in a large hypertrophic cardiomyopathy family with a single MYH7 mutation. *Sci. Rep.* **1**, 973
- Wang, B., Wang, J., Wang, L. F., Yang, F., Xu, L., Li, W. X., He, Y., Zuo, L., Yang, Q. L., Shao, H., Hu, D., and Liu, L. W. (2019) Genetic analysis of monoallelic double MYH7 mutations responsible for familial hypertrophic cardiomyopathy. *Mol. Med. Rep.* **6**, 5229–5238
- Li, B., Zhou, H., Wu, X., Chen, Z., and Yin, Y. (2016) Effects of dietary supplementation with uridine monophosphate on performance and intestinal morphology of weanling piglets. *J. Anim. Sci.* **7**, 82–86
- Zhang, X., Lin, Q., Chen, J., Wei, T., Li, C., Zhao, L., Gao, H., and Zheng, H. (2018) High Glucose-Induced Cardiomyocyte Death May Be Linked to

- Unbalanced Branched-Chain Amino Acids and Energy Metabolism. *Molecules* **4**, 807
29. Landoni, G., Zangrillo, A., Lomivorotov, V. V., Likhvantsev, V., Ma, J., De Simone, F., and Fominskiy, E. (2016) Cardiac protection with phosphocreatine: A meta-analysis. *Interact Cardiovasc. Thorac. Surg.* **4**, 637–646
 30. Elgebaly, S. A., Poston, R., Todd, R., Helmy, T., Almaghraby, A. M., Elbayoumi, T., and Kreutzer, D. L. (2019) Cyclocreatine protects against ischemic injury and enhances cardiac recovery during early reperfusion. *Expert Rev. Cardiovasc. Ther.* **9**, 683–697
 31. Guzun, R., Timohhina, N., Tepp, K., Gonzalez-Granillo, M., Shevchuk, I., Chekulayev, V., Kuznetsov, A. V., Kaambre, T., and Saks, V. A. (2011) Systems bioenergetics of creatine kinase networks: Physiological roles of creatine and phosphocreatine in regulation of cardiac cell function. *Amino Acids*. **5**, 1333–1348
 32. Dai, H., Chen, L., Gao, D., and Fei, A. (2019) Phosphocreatine Attenuates Isoproterenol-Induced Cardiac Fibrosis and Cardiomyocyte Apoptosis. *Biomed Res. Int.* **2019**, 5408289
 33. Guimarães-Ferreira, L. (2014) Role of the phosphocreatine system on energetic homeostasis in skeletal and cardiac muscles. *Einstein (Sao Paulo)*. **1**, 126–131
 34. O'Connor, R. S., Steeds, C. M., Wiseman, R. W., and Pavlath, G. K. (2008) Phosphocreatine as an energy source for actin cytoskeletal rearrangements during myoblast fusion. *J. Physiol.* **12**, 2841–2853
 35. Perepech, N. B., Nedoshivin, A. O., and Kutuzova, A. E. (1993) [Exogenous phosphocreatine in the prevention and treatment of cardiac insufficiency in patients with myocardial infarction]. *Klin Med. (Mosk)*. **1**, 19–22
 36. Krebs, H. A., and Johnson, W. A. (1980) The role of citric acid in intermediate metabolism in animal tissues. *FEBS Lett.* K1–K10
 37. Zdzisińska, B., Żurek, A., and Kandefer-Szerszeń, M. (2017) Alpha-ketoglutarate as a molecule with pleiotropic activity: Well-known and novel Possibilities of therapeutic Use. *Arch. Immunol. Ther. Exp. (Warsz)*. **1**, 21–36
 38. Karaman, S., Barnett, J., Jr., Sykes, G. P., Hong, B., and Delaney, B. (2011) Two-generation reproductive and developmental toxicity assessment of dietary N-acetyl-L-aspartic acid in rats. *Food Chem. Toxicol.* **12**, 3192–3205
 39. Teloh, J. K., Ansoorge, L., Petersen, M., Demircioglu, E., Waack, I. N., Brauckmann, S., Jakob, H., and Dohle, D. S. (2018) Histidine metabolism after Bretschneider cardioplegia in cardiac surgical patients. *Physiol. Res.* **67**, 209–216
 40. Sinkler, C. A., Kalpage, H., Shay, J., Lee, I., Malek, M. H., and Grossman, L. I. (2017) Tissue- and Condition-specific Isoforms of Mammalian Cytochrome C Oxidase Subunits: From Function to Human Disease. *Oxid. Med. Cell Longev.* **2017**, 1534056
 41. Sun, N., Youle, R. J., and Finkel, T. (2016) The mitochondrial basis of aging. *Mol. Cell* **5**, 654–666
 42. Skogestad, J., Aronsen, J. M., Tovsrud, N., Wanichawan, P., Hougen, K., Stokke, M. K., Carlson, C. R., Sjaastad, I., Sejersted, O. M., and Swift, F. (2020) Coupling of the Na⁺/K⁺-ATPase to Ankyrin B controls Na⁺/Ca²⁺ exchanger activity in cardiomyocytes. *Cardiovasc. Res.* **1**, 78–90
 43. Perez-Riverol, Y., Csordas, A., Bai, J., Bernal-Llinares, M., Hewapathirana, S., Kundu, D. J., Inuganti, A., Griss, J., Mayer, G., Eisenacher, M., Pérez, E., Uszkoreit, J., Pfeuffer, J., Sachsenberg, T., Yilmaz, S., et al. (2019) The PRIDE database and related tools and resources in 2019: Improving support for quantification data. *Nucleic Acids Res.* **47**, D442–D450